Mechanical and microstructural investigations of tungsten and doped tungsten materials produced via powder injection molding

Steffen Antusch [a,*], David E.J. Armstrong [b], T. Ben Britton [c], Lorelei Commin [a], James S.K.-L. Gibson [b], Henri Greuner [d], Jan Hoffmann [a], Wolfram Knabl [e], Gerald Pintsuk [f], Michael Rieth [a], Steve G. Roberts [b], Tobias Weingaertner [a]

[a] Institute for Applied Materials, Karlsruhe Institute of Technology, Karlsruhe, Germany
[b] Department of Materials, University of Oxford, Oxford, United Kingdom
[c] Department of Materials, Imperial College London, London, United Kingdom
[d] Max-Planck-Institut fuer Plasmaphysik, Garching, Germany
[e] PLANSEE SE, Reutte, Austria
[f] Institute for Energy Research, Forschungszentrum Juelich, Juelich, Germany

ARTICLE INFO

ABSTRACT

The physical properties of tungsten such as the high melting point of 3420°C, the high strength and thermal conductivity, the low thermal expansion and low erosion rate make this material attractive as a plasma facing material. However, the manufacturing of such tungsten parts by mechanical machining such as milling and turning is extremely costly and time intensive because this material is very hard and brittle.

Powder Injection Molding (PIM) as special process allows the mass production of components, the joining of different materials without brazing and the creation of composite and prototype materials, and is an ideal tool for scientific investigations.

This contribution describes the characterization and analyses of prototype materials produced via PIM. The investigation of the pure tungsten and oxide or carbide doped tungsten materials comprises the microstructure examination, element allocation, texture analyses, and mechanical testing via four-point bend (4-PB). Furthermore, the different materials were characterized by high heat flux (HHF) tests applying transient thermal loads at different base temperatures to address thermal shock and thermal fatigue performance. Additionally, HHF investigations provide information about the thermo-mechanical behavior to extreme steady state thermal loading and measurements of the thermal conductivity as well as oxidation tests were done.

Post mortem analyses are performed quantifying and qualifying the occurring damage with respect to reference tungsten grades by metallographic and microscopical means.

1. Introduction

The advantages of tungsten for example the high strength and thermal conductivity, the low thermal expansion, low tritium inventory and low erosion rate make it attractive to be used in a wide range of applications for future fusion power plants [1,2]. Unfortunately, tungsten is very brittle and the fabrication costs are high. At the Karlsruhe Institute of Technology (KIT) the manufacturing methods for the mass production of such tungsten parts are intensively investigated. Powder Injection Molding (PIM) is a fabrication process in powder metallurgy (PM) for shaping metals and ceramics to near net shapes with reasonably tight tolerance and a good surface finish [3]. This process enables the mass production of low cost, high performance components with complex geometries. Materials with high melting points such as tungsten or tungsten alloys could be effectively fabricated with this process. Furthermore, PIM can be used to join tungsten and doped tungsten materials without additional brazing or welding [4,5]. In this work, PIM was used to develop new materials and the material properties were investigated by different tests and analyses. All process parameters are in view of mass production aspects. The producing of suitable powder mixtures using mechanical alloying (MA) is time and cost intensive [6–8]. To produce parts

* Corresponding author. Tel.: +49 721 608 22553; fax: +49 721 608 22095.
E-mail address: steffen.antusch@kit.edu (S. Antusch).

Table 1
Used powders, particle sizes, prepared compositions, sintering temperatures and theoretical density after sintering.

Powder	Particle size (FSSS)	Prepared composition	Sintering Temperature (°C)	Theoretical density (%T.D.)
W	1.0 – 2.0 μm	(P_W1): Pure W	1800	< 96.0
		(P_W2): Pure W	2400	98.8
		(P_W3): Pure W	2600	99.0
Y_2O_3	< 1.50 μm	(P_O1): W-2Y_2O_3	2400	< 98.9
		(8.1 vol.% Y_2O_3)		
La_2O_3	< 2.50 μm	(P_O2): W-2La_2O_3	2400	< 98.7
		(5.7 vol.% La_2O_3)		
TiC	< 50 nm	(P_C1): W-1TiC	2400	98.8
		(3.8 vol.% TiC)		
TaC	< 1.0 μm	(P_C2): W-2TaC	2400	< 98.6
		(2.7 vol.% TaC)		
		(P_C3): W-8TaC	2400	< 98.5
		(10.7 vol.% TaC)		

Fig. 1. Finished PIM plate after heat-treatment and small test samples (produced via EDM).

in mass production a suitable method of producing the needed powders is necessary and alternative ways should be investigated. These new materials can be produced by mixing w/o mechanical alloying in order to save cost and time.

2. Experiment

2.1. Used powders, powder mixtures and feedstock preparation

The average particle size distribution of the used tungsten powder is in the range of 1.0–2.0 μm Fisher Sub-Sieve Size (FSSS). For the oxide doped tungsten materials lanthanum oxide (La_2O_3) powder (FSSS < 2.50 μm) and yttrium oxide (Y_2O_3) powder (FSSS < 1.50 μm) are used. For the carbide doped tungsten materials titanium carbide (TiC) powder (FSSS < 50 nm) and tantalum carbide (TaC) powder (FSSS < 1.0 μm) are used. All powders are mixed and different powder compositions prepared. For the composition of W-2La_2O_3 (P_O1), the tungsten powder particle system was doped with 2 wt.-% La_2O_3 powder and for W-2Y_2O_3 (P_O2) with 2 wt.-% Y_2O_3 powder. For the carbide doped tungsten materials the tungsten powder was doped with 1 wt.-% TiC powder (W-1TiC, (P_C1)), for W-2TaC (P_C2) with 2 wt.-% TaC powder, and for W-8TaC (P_C3) with 8 wt.-% TaC powder.

After heating at 80°C for removing moisture the powders are dry mixed to form the "feedstock" with a 50 vol.-% binder system, based on polyolefine, in a kneader. The finished granulated feedstock must be homogeneous and free from agglomeration.

2.2. Production of small prototype plates via PIM

The injection molding of the "green parts" (consisting of powder and binder) was carried out on an ELEKTRA injection molding machine. After injection molding the green parts were debound. During the debinding step not only the binder and the impurities (mainly O and C) are removed, but also the high residual stresses generated during injection molding are released. A subsequent heat-treatment process in dry H_2 for 2 h follows to finish the parts. All details (materials and sintering temperatures) are listed in Table 1. The theoretical density (T.D.) for the finished plates sintered at 2400°C is $\sim$ 99% T.D, and the shrinkage after the heat-treatment process is nearly 20%. Fig. 1 shows a finished plate after the heat-treatment process and the prepared (via electrical discharge machining, EDM) small samples for 4-point bending tests.

2.3. Characterization and testing methods

Material characterization was carried out to determine the homogeneity of the microstructure including impurity and elemental distribution. The mechanical properties of the materials were determined in order to assess strength and changes in ductility. Finally, the influence of high heat flux and oxidation tests was investigated. The microstructure of the different materials was examined using the secondary electron imaging of a focused ion beam cross-section, cut with a Zeiss AURIGA FIB. Auger electron spectroscopy (AES) with an Auger Nanoprobe PHI 680 (Physical Electronics, USA) was used to characterize the element allocation of tungsten and the oxide or carbide particles. To analyze the crystallographic texture a field emission scanning electron microscope Zeiss AURIGA CrossBeam Focused Ion Beam device with an EBSD detector was used. The detector collected the backscattered electrons from the sample which is used to determine grain orientation. Inverse pole figure maps were cleaned using a Grain Dilation algorithm with a tolerance angle of 5. Approximately 1% of the measure points were changed by the cleanup. Misorientations > 15° were considered a large angle grain boundary. Misorientations between 2 and 14° were considered sub-grain boundaries. Texture measurements were calculated using the original datasets after removing points with a confidence index below 0.1. On the small test samples the mechanical properties were measured with an INSTRON machine and 4-Point bending test rig. The thermal shock tests are carried out at JUDITH-1 (see chapter 3.5) and the high heat flux tests at GLADIS (see chapter 3.6). For the oxidation tests on pure tungsten a standard furnace was used.

3. Results

3.1. Microstructure of the developed materials

The microstructures are shown in Fig. 2. For pure tungsten (P_W1) a small grain size and many pores are visible. Here the sintering temperature was too low. This also agrees with the low density. P_W3 shows very large grains, in consequence of sintering at 2600°C. For all doped materials ($P_O1 – P_C3$) the embedded oxide and carbide particles (Y_2O_3, La_2O_3, TiC and TaC) are homogeneously embedded around the tungsten grain boundaries and act as grain growth inhibitor. Only the TaC doped materials (P_C2 and P_C3) showed agglomeration of the TaC particles in the several micrometer range.
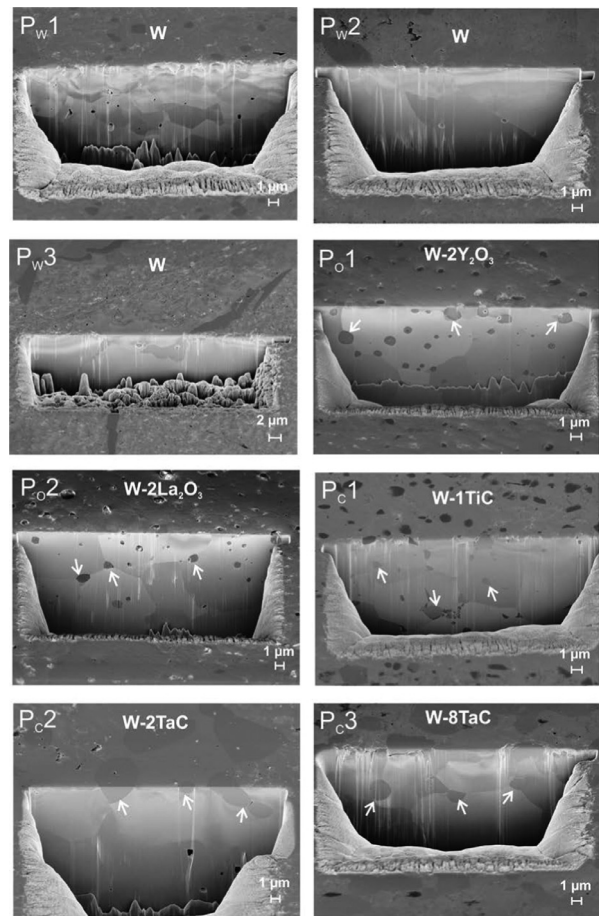

Fig. 2. SEM image of the microstructure for all samples performed via FIB. Some oxides and carbides are marked by arrows.

3.2. Element allocation (AES)

To determine the element allocation with AES, each sample was broken by a procedure after inward transfer into the machine. The samples are on a special ring under vacuum conditions to exclude other unwanted effects (dust or impurities) from the fresh broken fracture surface. Fig. 3–7 show the results for all oxide and carbide doped materials. It is clearly seen that the added elements are embedded around the tungsten grain boundaries. For the samples P_O1 and P_C1 (Figs. 3 and 5) the smallest grain size of all materials with around 4 μm was achieved. For the samples P_C2 and P_C3 (Figs. 6 and 7) the TaC grains form island-like structures. This means in comparison to the initial powder particle size, the tantalum carbide particles must be agglomerated.

3.3. Crystallographic texture (EBSD)

Electron backscatter diffraction (EBSD) is a powerful microstructural characterization tool in combination with an SEM and allows analyses e.g. of the crystal type [9]. All samples are polished with 20 nm colloidal silica and tilted at 70°. The resulting images are rotated at 180° and cleaned up. Fig. 8 shows the crystallographic orientations in normal direction (ND) for rolled tungsten produced by PLANSEE as reference and exemplarily for PIM pure tungsten (P_W2). Rolled tungsten as reference shows the typical grain oriented texture in rolling direction (A) due to the fabrication process. The beneficial material properties – e.g. high strength, bending toughness – are only achieved in the rolling direction. The EBSD texture of PIM tungsten is shown in (C). The texture is homogeneous and no preferred
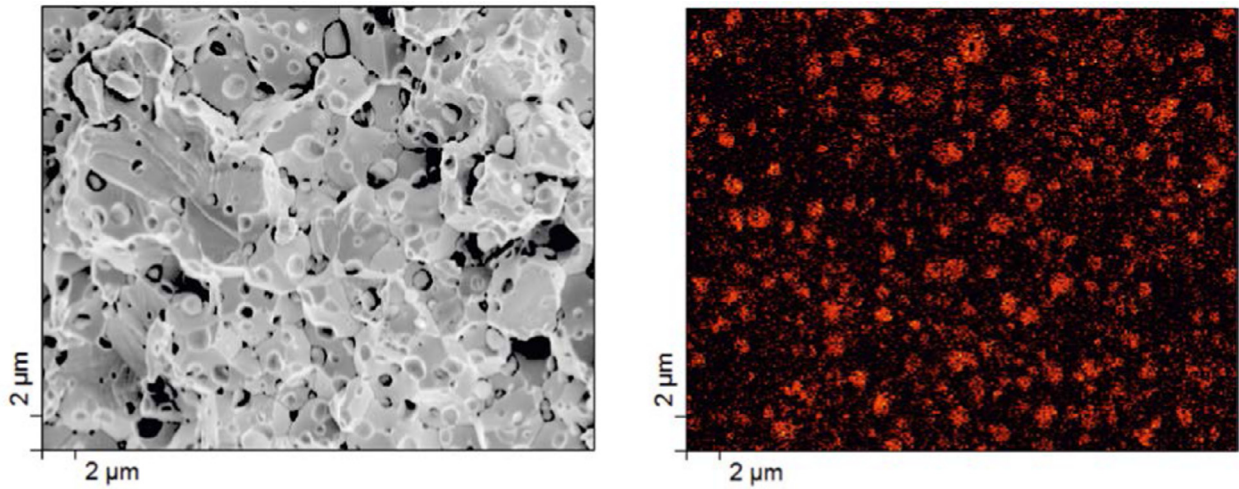
Fig. 3. Sample P_O1: SEM image of the fracture surface (left), and AES image of Y (in red color: Y, in black color: W matrix). (For interpretation of the references to color in this figure legend, the reader is referred to the web version of this article.)
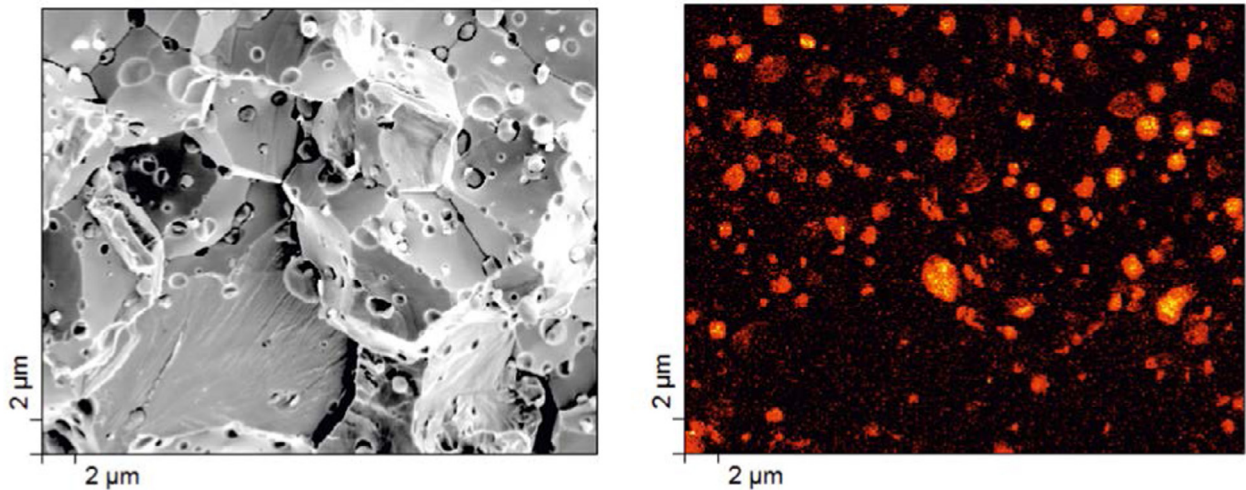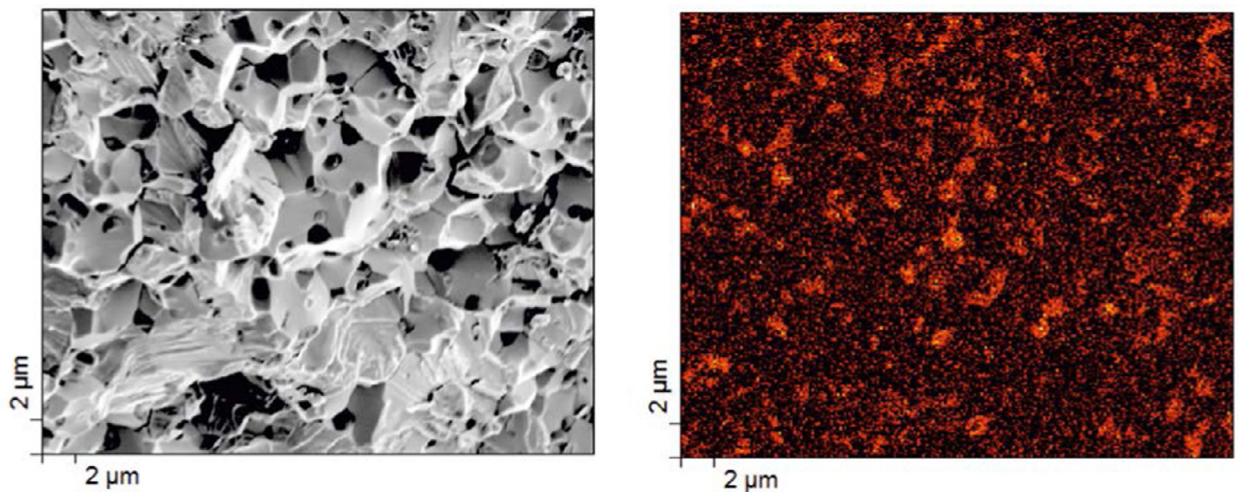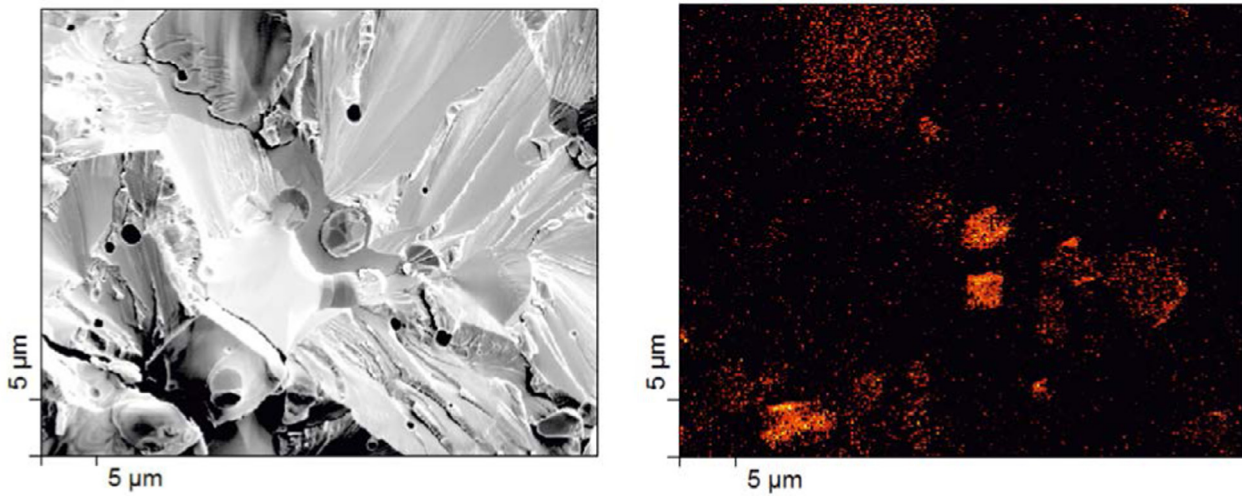

Fig. 4. Sample P_O2: SEM image of the fracture surface (left), and AES image of La (in red color: La, in black color: W matrix). (For interpretation of the references to color in this figure legend, the reader is referred to the web version of this article.)

Fig. 5. Sample P_C1: SEM image of the fracture surface (left), and AES image of Ti (in red color: Ti, in black color: W matrix). (For interpretation of the references to color in this figure legend, the reader is referred to the web version of this article.)
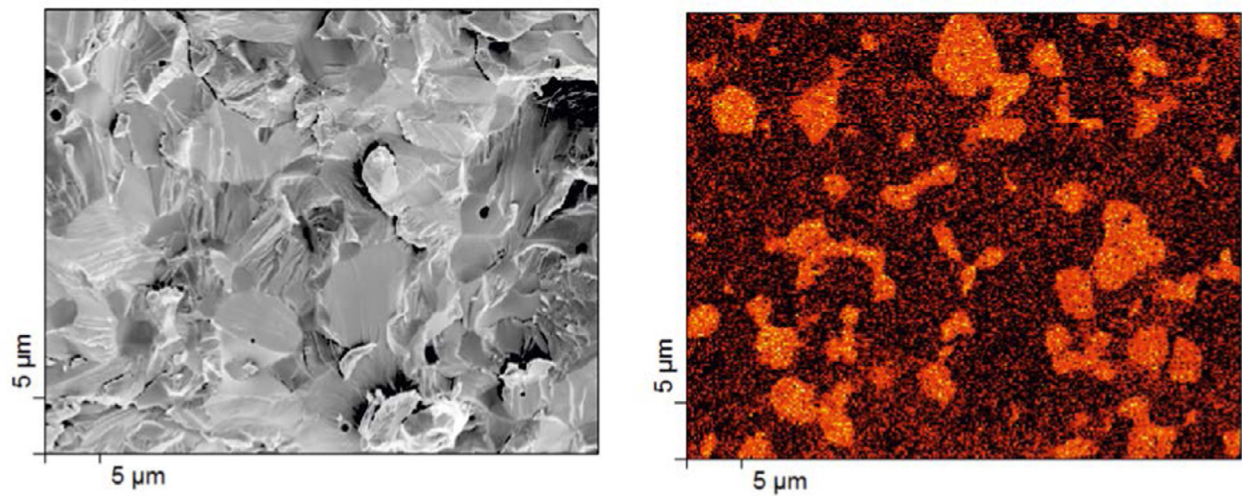
Fig. 6. Sample P_C2: SEM image of the fracture surface (left), and AES image of Ta (in red color: Ta, in black color: W matrix). (For interpretation of the references to color in this figure legend, the reader is referred to the web version of this article.)
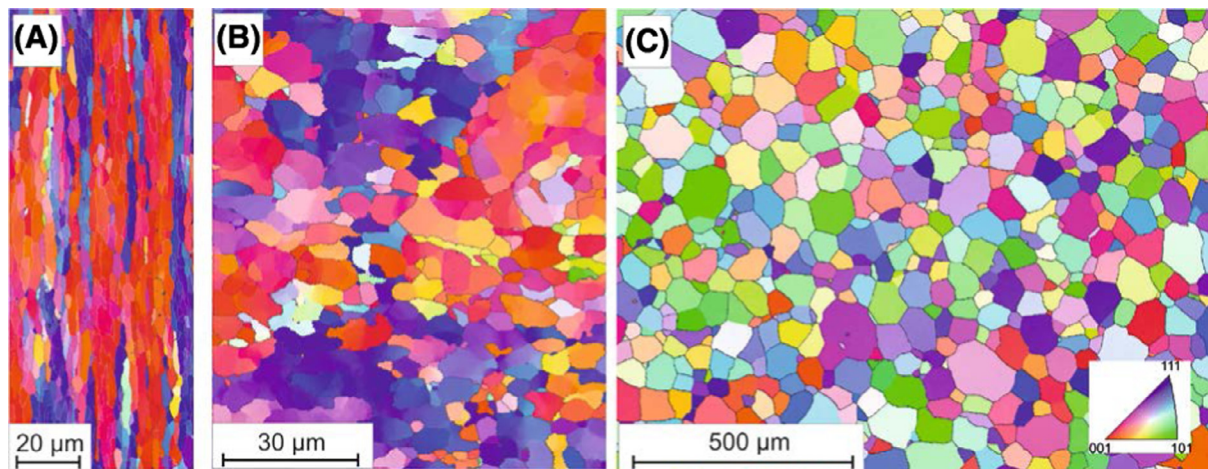

Fig. 7. Sample P_C3: SEM image of the fracture surface (left), and AES image of Ta (in red color: Ta, in black color: W matrix). (For interpretation of the references to color in this figure legend, the reader is referred to the web version of this article.)

Fig. 8. The crystallographic texture in the normal direction of rolled tungsten (Plansee): (A) in rolling direction; and (B) perpendicular to the rolling direction. The EBSD texture of PIM tungsten: (C) the material is fully anisotropic.
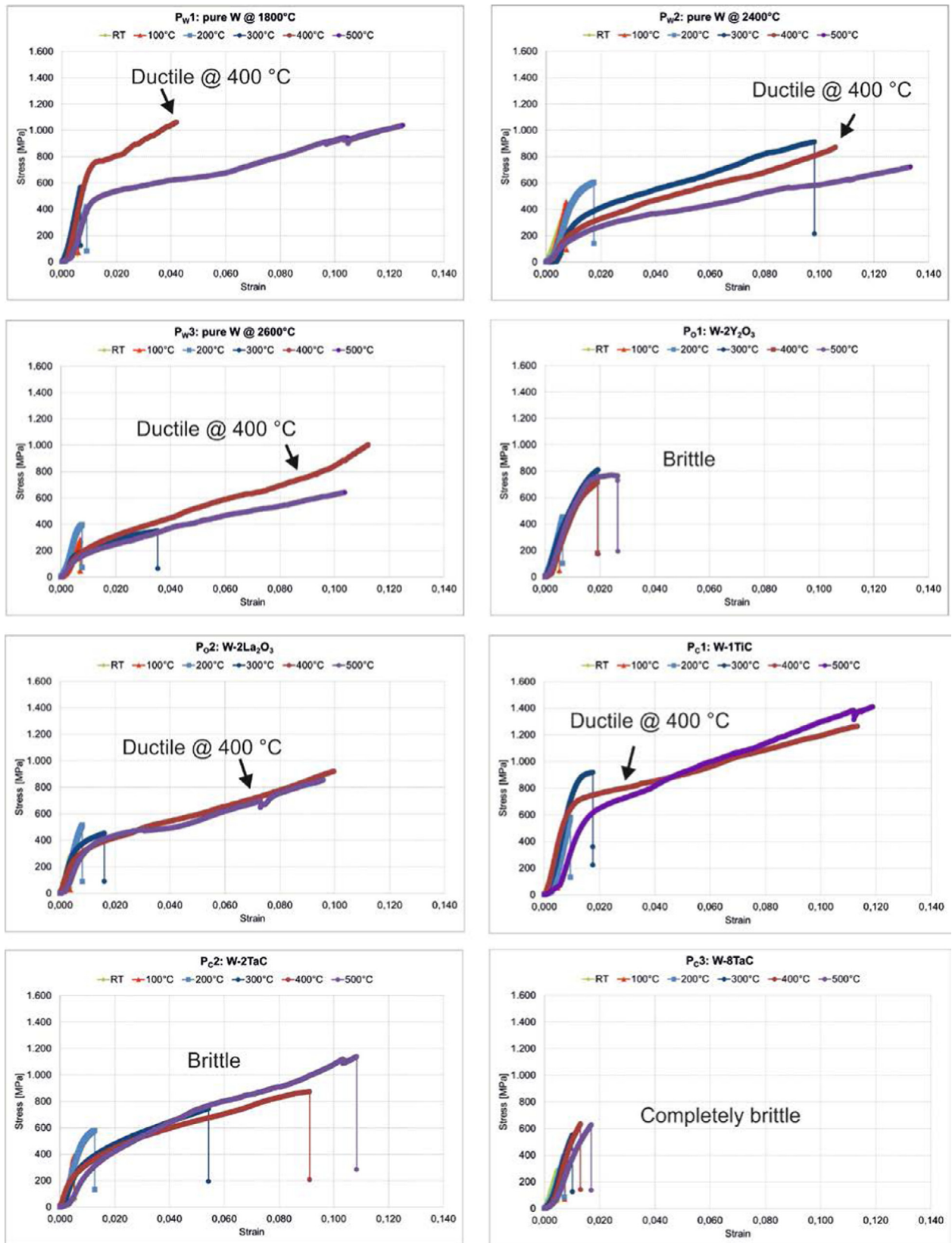
Fig. 9. Complete stress-strain curve for pure tungsten, tested from 20°C to 500°C.
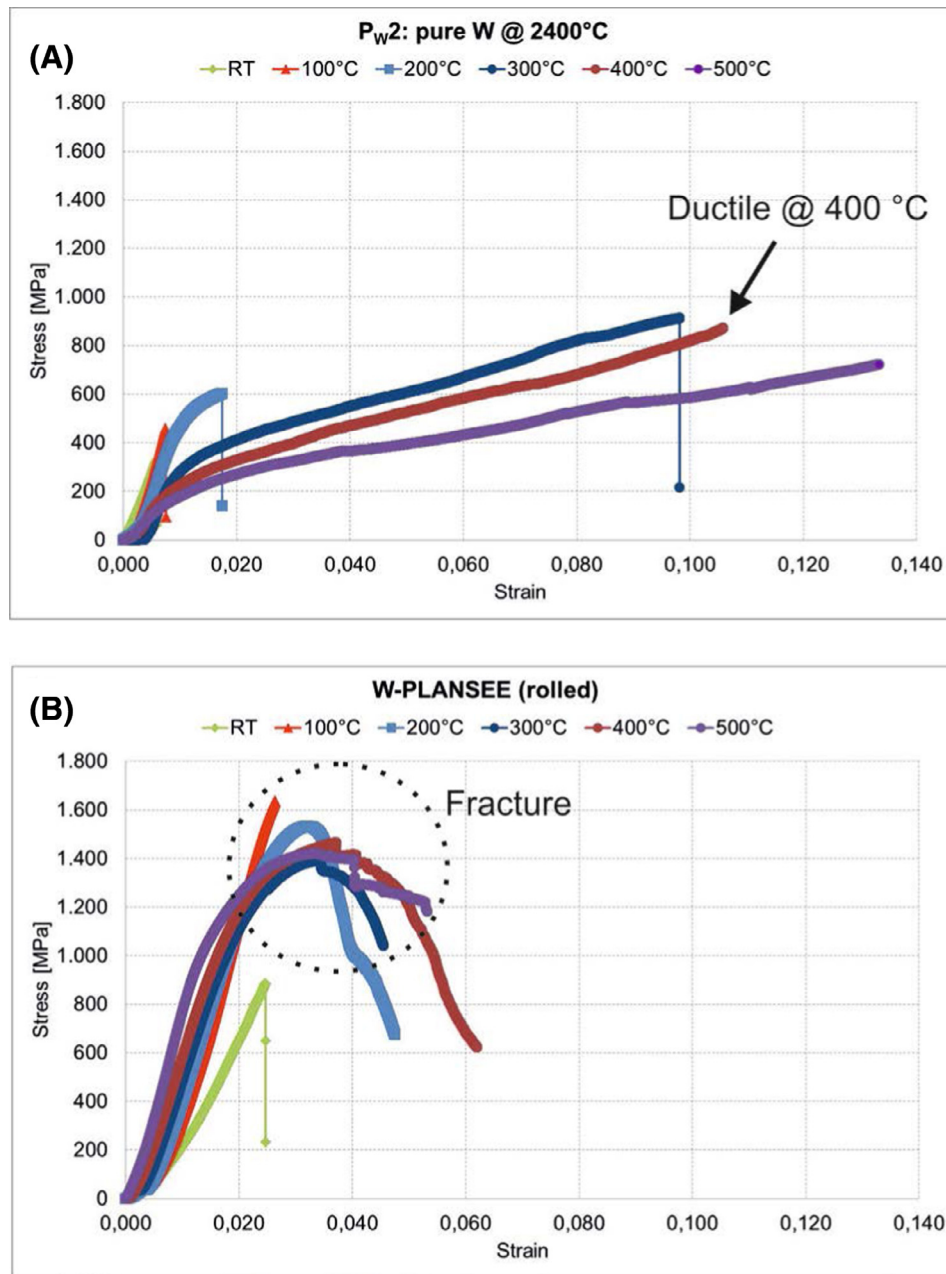
Fig. 10. Complete stress-strain curve, tested from 20°C to 500°C for pure PIM (P$_W$2) tungsten (A) and rolled PLANSEE tungsten (B).

orientation (as expected) is visible, the material is fully anisotropic. The results for the doped PIM tungsten materials are similar.

3.4. Mechanical testing via 4-point bending (4-PB) tests

To analyze the mechanical properties, in particular the brittle-to-ductile transition temperature (BDTT) and yield stress as a function of temperature, small samples of (12 × 1×1) mm were produced via the electrical discharge machining (EDM), see Fig. 1. After polishing of all four sides of each sample, all samples were notched via EDM. The 4-point bending tests were carried out on an INSTRON 3366 testing machine with a constant strain rate of 3.3E-05, with the cross-head velocity adjusted for each test to account for the different dimensions of each beam, at temperatures from 20°C to 500°C [10–12]. The raw load displacement data were then converted into stress-strain data. The results are shown in Fig. 9. The best results (microstructure, density and mechanical testing) for pure tungsten are achieved at a

sintering temperature of 2400°C (P$_W$2) which show ductility at 200°C as well as a higher yield stress than the material processed at 2600°C. All of the pure tungsten samples, W-2La$_2$O$_3$ and W-1TiC show brittle failure up to 350°C, while above 400°C no fracture was observed. W-2Y$_2$O$_3$, W-2TaC and W-8TaC are very brittle and fracture until 500°C, while the other materials show limited ductility before brittle fracture at lower temperatures. See exemplary pure PIM tungsten (P$_W$2) in comparison to rolled PLANSEE tungsten in Fig. 10. The rolled tungsten shows a very high stress level, but in comparison to the pure PIM tungsten less strain to failure indicating limited ductility in this material.

3.5. Thermal shock testing at JUDITH-1

At FZ Juelich high heat flux tests at the electron beam facility JUDITH-1 were performed applying transient thermal loads at different base temperatures to address thermal shock and thermal fatigue.

Table 2
Thermal-shock test parameters.

#	T [°C]	P_{abs} [GW/m²]	Δt [ms]	E_{abs} [MJ/m²]	FHF [MW/m²∗s$^{1/2}$]	# Shots
A	~ 20	0.38	1	0.38	12	1000
B	~ 20	1.13	5	5.67	80	100
C	1000	0.38	1	0.38	12	1000
D	1000	1.13	5	5.67	80	100

Loading condition: C
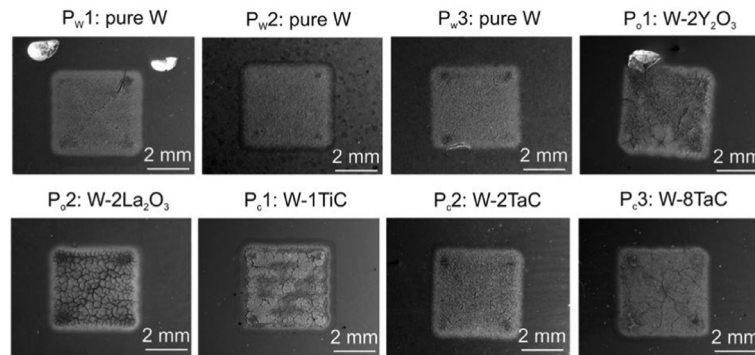
Fig. 11. Microstructure (surface) for all samples after loading condition C.
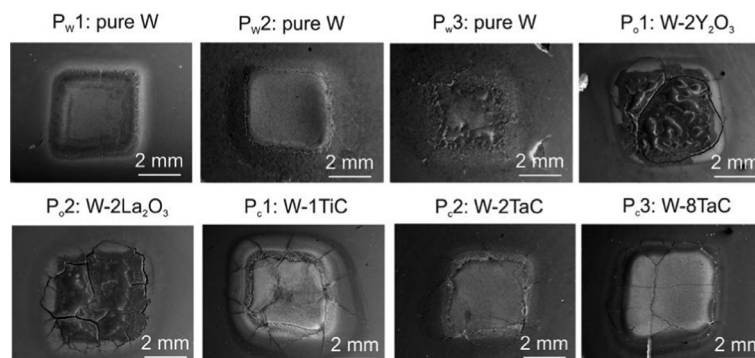
Loading condition: D

Fig. 12. Microstructure (surface) for all samples after loading condition D.

Post-mortem analyses to quantify and qualify the occurring damage with respect to reference tungsten grades were done by the SEM observation of the loaded area. Table 2 shows the testing parameter for all samples and Figs. 11–13 the microstructure of the samples after testing. The best result after the thermal load testing is achieved for pure tungsten sintered at 2400°C (P_W2), see Fig. 13. Only a rough surface, but no cracks are visible. The other pure tungsten samples (P_W1, P_W3), all oxide and carbide doped tungsten materials and the single forged pure tungsten (as reference, produced by PLANSEE) show cracks or damage after the test.

3.6. HHF testing at GLADIS

The Garching LArge DIvertor Sample test facility (GLADIS) at IPP Garching serves for investigating the thermo-mechanical behavior of components subjected to extreme thermal loading. The facility is equipped with 2 MW neutral beams for homogeneous heating of plasma facing components at heat fluxes up to 90 MW/m² and 45 s pulse length [13]. The aims of the HHF tests of pure PIM W mock-ups are: (1) a study of thermo-mechanical behavior (temporally-resolved
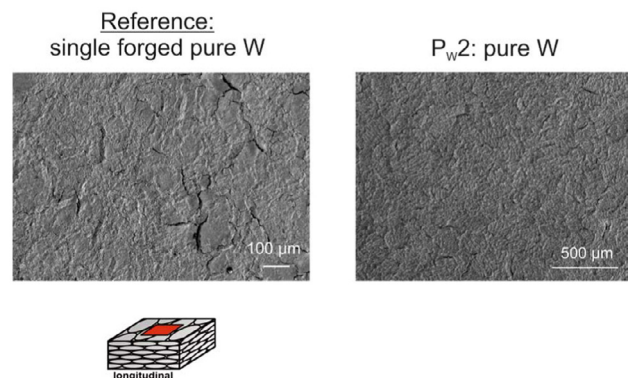
Loading condition: C

Fig. 13. Microstructure (surface) for pure tungsten PIM (P_W2) in comparison with single forged pure tungsten after loading condition C.
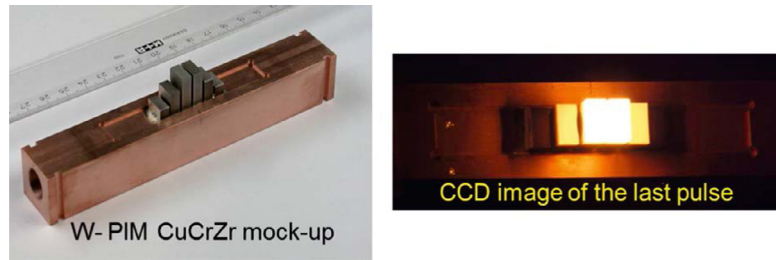
Fig. 14. The W-PIM CuCrZr mockup before (left), and during the tests (right) at GLADIS.

surface temperature evolution during screen and cycling) and (2) a study of surface morphology changes due to high temperature and high H fluxes (grain growth, porosity, and surface structure). Some pre-tests on the PIM material show promising results [14]. Fig. 14 shows the W PIM CuCrZr-mockup before and during the tests. Pure PIM tungsten (P_W2) was used as a test material. The surface after the cyclic loading is rough and some thermal fatigue cracks in the range of 10–15 μm on the surface are visible (see Fig. 15). The pure PIM W material showed good thermal performance, withstanding without defects the 10 MW/m² cyclic loading.

Additionally to the HHF testing measurements of the thermal conductivity were done by laser flash (Fig. 16). The results for the PIM pure W (average of sample 1 and sample 2 in red color) are under the ITER database curve (blue color). This shows the quality of the PIM process to produce parts with the required thermal conductivity λ. No surface temperature (T_{surf}) increases during cycling were measured and the overall performance was very stable.

3.7. Oxidation tests on pure W

The oxidation tests were carried out on pure PIM tungsten (P_W2) in comparison with rolled tungsten produced by PLANSEE. Fig. 17 shows the results of both materials. The rolled pure tungsten plate shows complete failure and unstable collapse after 48 h at the furnace (600°C, air atmosphere). In contrast the shape of the pure PIM tungsten part "tile" is well preserved after 4 days at the furnace (700°C, air atmosphere).
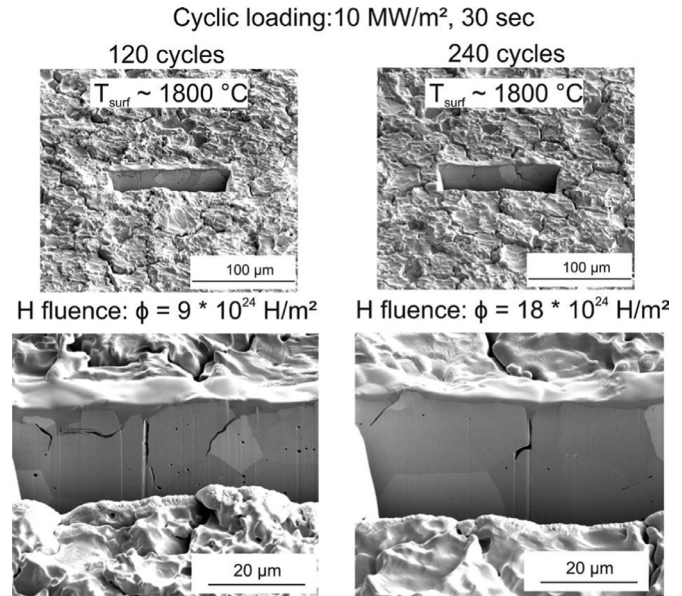

Fig. 15. The microstructure of W-PIM sample P_W2 after 120 cycles (left), and after 240 cycles (right) at GLADIS.
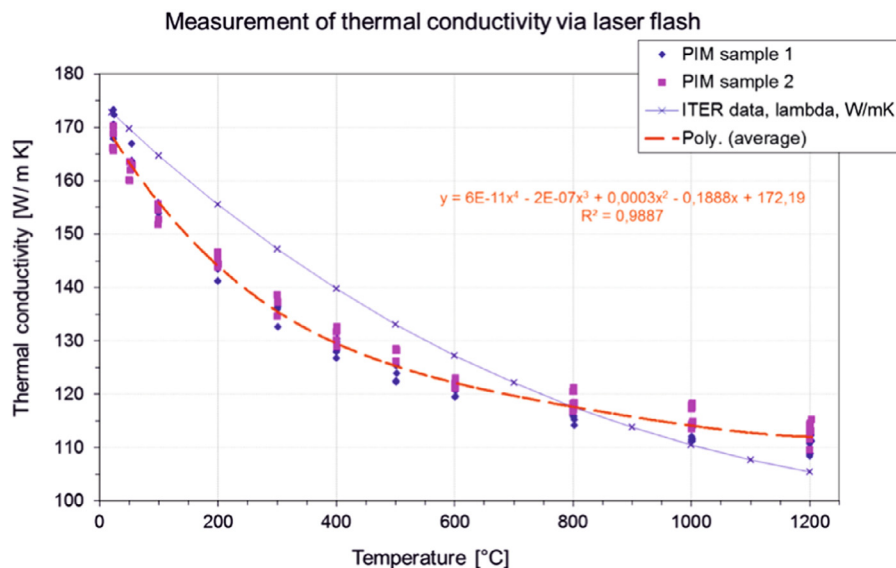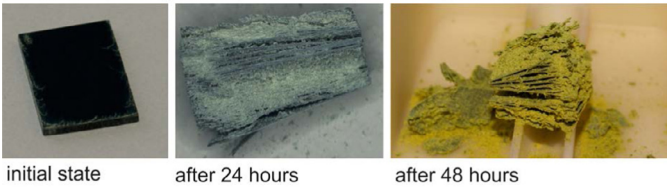

Fig. 16. Measurement of the thermal conductivity via laser flash measurement.

Reference: rolled pure W plate: 600 °C, air atmosphere

initial state   after 24 hours   after 48 hours

Pure tungsten PIM part „tile": 700 °C, air atmosphere
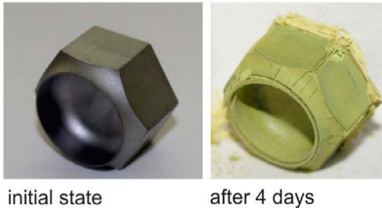

initial state   after 4 days

Fig. 17. Oxidation tests on pure tungsten.

4. Discussion

The motivation for this work was the investigation of prototype materials produced by PIM. The microstructure of the finished doped tungsten materials showed a homogeneous allocation of the embedded particles. The elemental allocation was similarly well-distributed. Therefore, we can conclude that the production of the materials solely by mixing was successful. This allows a great saving in cost and time in the subsequent process chain. The mechanical tests show that sintering at 2400°C produces the best results for pure tungsten, (P_W2). Also the microstructure looks homogeneous, and the density is high (~99% T.D.). In comparison to rolled tungsten produced by PLANSEE, the crystallite orientation of all PIM tungsten materials is random. The addition of 1wt-% TiC into the tungsten matrix produces a stronger material, without any detrimental effect on the ductility or brittle-to-ductile transition temperature (BDTT). TaC seems to be even more agglomerated (as larger initial particles were used). This could be avoided by mechanical alloying, but the process costs will be increased [15]. In the oxide and carbide doped materials, the tungsten grains are small, because the embedded particles (Y_2O_3, La_2O_3, TiC) act as grain growth inhibitors. W-2Y_2O_3, W-2TaC and W-8TaC show very brittle behavior. The content of the oxide and carbide addition (see Table 1) is too high in these materials and has to be adapted.

Despite the improvements seen in four-point bend tests, only pure tungsten sintered at 2400°C (P_W2) performed well under thermal shock loading. The other pure tungsten samples (P_W1, P_W3) and all oxide and carbide doped tungsten materials show cracks or damage after the test. As a result, for the HHF test at GLADIS only the pure PIM W material (P_W2) was used, despite the original intention to characterize all samples. This material showed good thermal performance and withstood without defects the 10 MW/m² cyclic loading. This was determined through the measurement of the thermal conductivity with no surface temperature increase T_{surf} during cycling.

Also the results of the oxidation test are very promising. Rolled tungsten has grain boundaries in rolling direction. Oxygen diffuses on these grain boundaries and the layers diverge like a flaky pastry. A possible explanation why PIM tungsten is more stable could be the uniaxial grain orientation. PIM tungsten materials show a homogeneous grain structure without rolling texture and therefore, the oxi-

dation is evenly distributed within the volume. The rolling materials have a larger grain boundary surface and offer more (approximately 1 to 2 magnitudes) space for oxidation.

Summarized, the results show that pure PIM tungsten exhibits some interesting properties that are very important for the continuation of this work. The content of oxide and carbide doped materials must be improved and further investigations will deliver more information about the properties of materials produced via PIM.

5. Conclusions and outlook

The advantage of tungsten materials produced via PIM is not the strength. Rolled, swaged or forged tungsten materials produced by PLANSEE will deliver much better results. However PIM is a powerful process for mass production of near net shape parts. This method can also be used to create new materials relatively fast in order to investigate their properties. This will be more in focus at KIT for further work and investigations. The interesting questions are: which parameters have an influence on the material properties and how to study them. This work shows that in addition to the sintering temperature and time, the type, size, and concentration of the doping particles have an enormous effect on the material properties and will be investigated in the future.

References

[1] M. Rieth, S.L. Dudarev, S.M. Gonzalez de Vicente, J. Aktaa, T. Ahlgren, S. Antusch, D.E.J. Armstrong, et al., J. Nucl. Mater. 432 (2013) 482–500.
[2] R.A. Pitts, S. Carpentier, F. Escourbiac, T. Hirai, V. Komarov, S. Lisgo, A.S. Kukushkin, A. Loarte, A. Merola, A. Sashala Naik, R. Mitteau, M. Sugihara, B. Bazylev, P.C. Stangeby, J. Nucl. Mater. 438 (2013) 48–56.
[3] R.M. German, *Metal Injection Molding*, Metal Powder Industries Federation, Princeton, NJ, 2011, pp. 20–33.
[4] S. Antusch, V. Piotter, Powder Injection Molding Int. 6 (2012).
[5] S. Antusch, L. Commin, J. Heneka, V. Piotter, K. Plewa, H. Walter, Fusion Eng. Des. 88 (2013) 2461–2465.
[6] S.C. Cifuentes, A. Muñoz, M.A. Monge, P. Pérez, J. Nucl. Mater. 442 (2013) 214–S218.
[7] A. Muñoz, M.A. Monge, B. Savoini, M.E. Rabanal, G. Garces, R. Pareja, J. Nucl. Mater. 417 (2011) 508–511.
[8] P. López-Ruiz, N. Ordás, I. Iturriza, M. Walter, E. Gaganidze, S. Lindig, F. Koch, C. García-Rosales, J. Nucl. Mater. 442 (2013) 219–224.
[9] A.J. Wilkinson, T.B. Britton, Strains, Mater. Today 15 (9) (2012) 366–376.
[10] A. Giannattasio, Z. Yao, E. Tarleton, S.G. Roberts, Philos. Mag. 90 (30) (2010) 3947–3959.
[11] A. Giannattasio, M. Tanaka, T.D. Joseph, S.G. Roberts, Phys. Scr. T 128 (2007) 87–90.
[12] A. Giannattasio, S.G. Roberts, Philos. Mag. 87 (17) (2008) 2589–2598.
[13] H. Greuner, B. Boeswirth, J. Boscary, P. McNeely, et al., J. Nucl. Mater. 367–370 (2007) 1444–1448.
[14] H. Greuner, H. Maier, M. Balden, Ch. Linsmeier, B. Böswirth, S. Lindig, P. Norajitra, S. Antusch, M. Rieth, J. Nucl. Mater. 442 (2013) 256–260.
[15] H.H. Kurishita, Y. Amano, S. Kobayashi, K. Nakai, H. Arakawa, Y. Hiraoka, T. Takida, K. Takebe, H. Matsui, J. Nucl. Mater. 367–370 (2007) 1453–1457.